

Article

LaNi₅-Assisted Hydrogenation of MgNi₂ in the Hybrid Structures of La_{1.09}Mg_{1.91}Ni₉D_{9.5} and La_{0.91}Mg_{2.09}Ni₉D_{9.4}

Roman V. Denys¹, Volodymyr A. Yartys^{1,2,*}, Evan MacA. Gray³ and Colin J. Webb³

¹ Institute for Energy Technology, P.O. Box 40, Kjeller NO 2027, Norway;
E-Mail: roman.v.denys@gmail.com

² Norwegian University of Science and Technology, Trondheim NO 7491, Norway

³ Queensland Micro- and Nanotechnology Centre, Griffith University, Nathan 4111, Brisbane, Australia; E-Mails: e.gray@griffith.edu.au (E.M.G.); j.webb@griffith.edu.au (C.J.W.)

* Author to whom correspondence should be addressed; E-Mail: volodymyr.yartys@ife.no;
Tel.: +47-454-22-065.

Academic Editor: Craig M. Jensen

Received: 26 February 2015 / Accepted: 13 April 2015 / Published: 21 April 2015

Abstract: This work focused on the high pressure PCT and *in situ* neutron powder diffraction studies of the LaMg₂Ni₉-H₂ (D₂) system at pressures up to 1,000 bar. LaMg₂Ni₉ alloy was prepared by a powder metallurgy route from the LaNi₉ alloy precursor and Mg powder. Two La_{3-x}Mg_xNi₉ samples with slightly different La/Mg ratios were studied, La_{1.1}Mg_{1.9}Ni₉ (sample 1) and La_{0.9}Mg_{2.1}Ni₉ (sample 2). *In situ* neutron powder diffraction studies of the La_{1.09}Mg_{1.91}Ni₉D_{9.5} (1) and La_{0.91}Mg_{2.09}Ni₉D_{9.4} (2) deuterides were performed at 25 bar D₂ (1) and 918 bar D₂ (2). The hydrogenation properties of the (1) and (2) are dramatically different from those for LaNi₃. The Mg-containing intermetallics reversibly form hydrides with $\Delta H_{des} = 24.0$ kJ/molH₂ and an equilibrium pressure of H₂ desorption of 18 bar at 20 °C (La_{1.09}Mg_{1.91}Ni₉). A pronounced hysteresis of H₂ absorption and desorption, ~100 bar, is observed. The studies showed that LaNi₅-assisted hydrogenation of MgNi₂ in the LaMg₂Ni₉ hybrid structure takes place. In the La_{1.09}Mg_{1.91}Ni₉D_{9.5} (1) and La_{0.91}Mg_{2.09}Ni₉D_{9.4} (2) (a = 5.263/5.212; c = 25.803/25.71 Å) D atoms are accommodated in both Laves and CaCu₅-type slabs. In the LaNi₅ CaCu₅-type layer, D atoms fill three types of interstices; a deformed octahedron [La₂Ni₄], and [La(Mg)₂Ni₂] and [Ni₄] tetrahedra. The overall chemical compositions can be presented as LaNi₅H_{5.6/5.0} + 2*MgNi₂H_{1.95/2.2} showing that the hydrogenation of the MgNi₂ slab proceeds at

mild H₂/D₂ pressure of just 20 bar. A partial filling by D of the four types of the tetrahedral interstices in the MgNi₂ slab takes place, including [MgNi₃] and [Mg₂Ni₂] tetrahedra.

Keywords: *in situ* studies; neutron powder diffraction; metal hydrides; lanthanum; magnesium

1. Introduction

Despite significant differences in chemistry between La and Mg, magnesium forms a very extensive solid solution in the LaNi₃ intermetallic alloy, crystallizing with a PuNi₃ type trigonal structure. Up to 67% of La atoms can be replaced by Mg to form a LaMg₂Ni₉ intermetallic compound. The LaNi₃ crystal structure is formed by a stacking of the LaNi₅ (*Haucke* CaCu₅ type) and MgNi₂ (*Laves* type) slabs along the trigonal 00z axis (LaNi₅ + 2MgNi₂ = LaMg₂Ni₉). Studies of hydrogen absorption–desorption properties of the LaMg₂Ni₉ [1,2] have shown that it forms a hydride containing up to 1.2 wt% H (~0.8 H/M; LaMg₂Ni₉H_{9.6}).

The building blocks of LaMg₂Ni₉—LaNi₅ and MgNi₂—are well characterized individually as hydride-forming intermetallic compounds. The thermodynamics and structural features of their interaction with hydrogen are quite different. At room temperature, LaNi₅ forms a saturated LaNi₅H_{6.7} hydride and shows a reversible interaction with hydrogen at hydrogen pressures slightly exceeding atmospheric pressure. Hydrogen atoms fill tetrahedral La₂Ni₂, LaNi₃ and Ni₄ sites in the hydride crystal structure [3].

In contrast, hydrogenation of the Laves phase MgNi₂ compound is possible only at hydrogen pressures close to 30 kbar, while maintaining an interaction temperature of 300 °C. Formation of MgNi₂H₃ results in a complete rebuilding of the metal sublattice. Hydrogen atoms in the orthorhombic structure of trihydride fill two different sites, the Mg₄Ni₂ octahedra and the positions within the buckled Ni nets, consequently forming directional Ni-H bonds [4].

A gradual increase of Mg content in La_{3-x}Mg_xNi₉ is accompanied by a linear decrease of the volumes of the unit cells. Interestingly, a substantial contraction takes place not only for the (La,Mg)₂Ni₄ slabs, but also for Mg-free CaCu₅-type LaNi₅ slabs. Hydrogen interaction with the La_{3-x}Mg_xNi₉ alloys has been investigated by *in situ* synchrotron X-ray, neutron powder diffraction, theoretical modeling, electrochemical studies as metal hydride battery anode materials, rapid solidification and pressure–composition–temperature studies [1,2,5–10]. In the whole substitution range, La_{3-x}Mg_xNi₉ alloys form intermetallic hydrides with H/M ratios ranging from 0.77 to 1.16. Magnesium influences structural features of the hydrogenation process and determines various aspects of the hydrogen interaction with intermetallics causing: (a) more than a 1,000-fold increase in the equilibrium pressures of hydrogen absorption and desorption for the Mg-rich LaMg₂Ni₉ as compared to the Mg-poor La_{2.3}Mg_{0.7}Ni₉ and a substantial modification of the thermodynamics of the formation–decomposition of the hydrides; (b) an increase of the reversible hydrogen storage capacities following increase of Mg content in the La_{3-x}Mg_xNi₉ to ~1.5 wt% H for La₂MgNi₉; (c) improvement of the resistance against hydrogen-induced amorphisation and disproportionation and (d) change of the mechanism of the hydrogenation from anisotropic to isotropic. Thus, optimisation of the magnesium

content provides different possibilities for improving properties of the studied alloys as hydrogen storage and battery electrode materials. Studies of the thermodynamics and crystal chemistry of the $\text{RE}_2\text{MgNi}_9\text{H}_{12-13}$ (RE = La and Nd) hydrides showed that La substitution by Pr or Nd causes destabilization of the formed hydrides without affecting their hydrogen storage capacities and leaves unchanged the most important features of their crystal structures [11].

Observed values of H capacities in the LaMg_2Ni_9 -based hydride of 9.6 atoms H/f.u. cannot be explained by exclusive hydrogen insertion into the LaNi_5 slabs, and requires H incorporation into the MgNi_2 blocks of the structure to reach the experimentally observed H/M ratios. Thus, studies of the thermodynamics and crystal chemistry of $\text{La}_{3-x}\text{Mg}_x\text{Ni}_9\text{-H}_2$ systems are very interesting and important from the point of view of the effect of magnesium on the behaviours of the metal-hydrogen systems. The goal of the present study was to study two alloy compositions formed close to the limiting value of the magnesium solubility in LaNi_3 , LaMg_2Ni_9 , by performing *in situ* neutron powder diffraction studies of the deuterated $\text{La}_{0.91}\text{Mg}_{2.09}\text{Ni}_9$ and $\text{La}_{1.09}\text{Mg}_{1.91}\text{Ni}_9$ and by studying the thermodynamics of the metal-hydrogen interactions by measurements of the PCT diagrams.

2. Experimental

$\text{La}_{1.09}\text{Mg}_{1.91}\text{Ni}_9$ and $\text{La}_{0.91}\text{Mg}_{2.09}\text{Ni}_9$ alloys were prepared by a powder metallurgy route from LaNi_5 alloy precursor, Mg and Ni. Initial metals La, Mg and Ni with high purity exceeding 99.9% were used in the synthesis. LaNi_5 precursor was prepared by arc melting of a stoichiometric 1:5 mixture of La and Ni.

The powder mixture $\text{LaNi}_5 + \text{Mg} + \text{Ni}$ was ball milled under protective atmosphere of argon gas in a SPEX 8000D mill for 8 h. After the milling process, the mixture was placed into a tantalum crucible and then annealed in Ar atmosphere in the sealed stainless steel containers at 600–1000 °C. Two samples with a slightly different stoichiometry were prepared. Their stoichiometric compositions were: sample 1: $\text{La}_{1.09(1)}\text{Mg}_{1.91(1)}\text{Ni}_9$; sample 2: $\text{La}_{0.91(1)}\text{Mg}_{2.09(1)}\text{Ni}_9$.

The first sample was annealed at 800 °C for 8 h and then at 600 °C for 8 h. The second sample was annealed at 1000 °C for 2 h and, later, at 800 °C for 12 h. The samples were quenched into a mixture of water and ice after the annealing. A small excess of Mg (5 wt%) was introduced into the initial mixtures to compensate for its sublimation at high temperatures.

The homogeneity of the prepared samples was characterized by XRD. Laboratory powder X-ray diffraction data were collected with a Siemens D5000 diffractometer (Oslo, Norway) equipped with a Ge primary monochromator giving $\text{Cu K}\alpha_1$ radiation. Initial phase-structural analysis was performed by X-ray powder diffraction using a Bruker D8 Advance diffractometer (Kjeller, Norway) with $\text{Cu-K}\alpha$ radiation. High-resolution SR XRD data were collected at the Swiss-Norwegian Beamlines (SNBL, BM01B) at ESRF, Grenoble, France. A monochromatic beam with $\lambda = 0.5009(1)$ Å was provided by a double Si monochromator. A 2θ angular range of 1°–50.5° was scanned with a detector bank consisting of six scintillation detectors mounted in series with 1.1° separation. The data were binned to the step size $\Delta 2\theta = 0.003^\circ$. The instrumental contribution to the line broadening was evaluated by refining the profile parameters for a standard Si sample.

In situ neutron powder diffraction studies were performed at HRPT diffractometer, SINQ, PSI, Switzerland using a wavelength of $\lambda = 1.494$ Å. The deuteride of sample 1 was synthesized at 25 bar

D₂ and $-30\text{ }^{\circ}\text{C}$ (P_{eq} for absorption ~ 20 bar); it was synthesized and studied by NPD using a thin walled stainless steel sample cell (6 mm OD). The deuteride of sample 2 was synthesized at 950 bar D₂ and measured at 912 bar D₂ at room temperature. The experimental setup for the *in situ* NPD study consisted of a high-pressure Sieverts' manometric hydrogenator connected to a high-pressure sample cell made of a null matrix coherent scattering alloy (Zr–Ti) with a thin stainless steel inner liner.

Powder diffraction data were analysed by the Rietveld whole-profile refinement method using the General Structure Analysis System (GSAS) [12] and FULLPROF [13] software packages. Pressure-composition-temperature isotherms were measured at -40 , -20 , 0 and $20\text{ }^{\circ}\text{C}$.

3. Results and Discussion

3.1. XRD Characterization of the Initial Intermetallic Alloys $\text{La}_{0.91}\text{Mg}_{2.09}\text{Ni}_9$ and $\text{La}_{1.09}\text{Mg}_{1.91}\text{Ni}_9$

XRD characterization of two studied alloys $\text{La}_{0.91}\text{Mg}_{2.09}\text{Ni}_9$ and $\text{La}_{1.09}\text{Mg}_{1.91}\text{Ni}_9$ showed that they both contain PuNi_3 trigonal $\text{La}_{3-x}\text{Mg}_x\text{Ni}_9$ as the main phase constituents (80% for sample 1 and 75% for sample 2). The common secondary constituent was identified as a LaNi_5 binary intermetallic. Furthermore, sample 1 contained an admixture of the MgNi_2 Laves-type intermetallic phase, while sample 2 contained a cubic MgNi_3 intermetallic compound recently also observed during the studies of the $\text{MgNi}_2\text{-H}_2$ system [4]. MgNi_3 compound (sp.gr. $Pm\bar{3}m$; $a = 3.7185(5)\text{ \AA}$) has an AlCu_3 -type structure and earlier it was synthesized by high-energy ball milling of a mixture of Mg and Ni metals [14]. We assume that in present study MgNi_3 was synthesised already during the reactive ball milling and remained stable during the consecutive annealing at $1,000$ and $800\text{ }^{\circ}\text{C}$. As an example, Figure 1 shows an excellent fit of the experimental X-ray powder diffraction pattern collected for the sample 2, $\text{La}_{0.91}\text{Mg}_{2.09}\text{Ni}_9$.

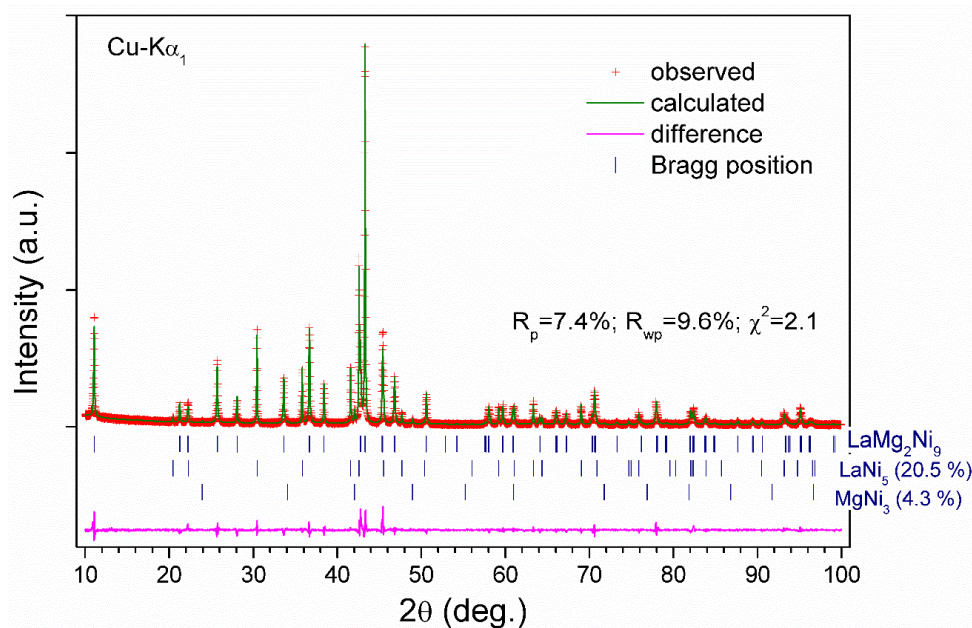


Figure 1. XRD pattern of $\text{La}_{0.91}\text{Mg}_{2.09}\text{Ni}_9$ (sample 2) ($\text{Cu-K}\alpha_1$ radiation).

Crystallographic data for the studied intermetallic samples obtained from the refinements of the XRD pattern are listed in Table 1.

Table 1. Crystal structure data for the La_{0.91}Mg_{2.09}Ni₉ and La_{1.09}Mg_{1.91}Ni₉ alloys from Rietveld refinements of the X-ray diffraction data. *PuNi₃* type of structure, space group $R\bar{3}m$.

Alloy	Sample 1	Sample 2
Source of experimental data	SR XRD collected at BM01B, SNBL using a wavelength $\lambda = 0.5009(1)$ Å	Siemens D5000 diffractometer, Cu K α_1 radiation
Composition of AB ₃ phase	La _{1.09(1)} Mg _{1.91(1)} Ni ₉	La _{0.91(1)} Mg _{2.09(1)} Ni ₉
Unit cell parameters:		
<i>a</i> (Å)	4.94024(8)	4.8986(1)
<i>c</i> (Å)	23.8188(4)	23.957(1)
<i>V</i> (Å ³)	503.44(1)	497.86(2)
Atomic parameters:		
La1/Mg1 in 3 <i>a</i> (0, 0, 0)		
<i>U</i> _{iso} × 100 (Å ²)	0.43(5)	2.1(2)
<i>n</i> _{Mg} , (<i>n</i> _{La} = 1 − <i>n</i> _{Mg})	0.0(−)	0.09(1)
La2/Mg2 in 6 <i>c</i> (0, 0, <i>z</i>)		
<i>z</i>	0.1453(3)	0.1471(6)
<i>U</i> _{iso} × 100 (Å ²)	1.2(3)	0.5(3)
<i>n</i> _{Mg} , (<i>n</i> _{RE} = 1 − <i>n</i> _{Mg})	0.954(5)	1.0(−)
Ni1 in 3 <i>b</i> (0, 0, ½)		
<i>U</i> _{iso} × 100 (Å ²)	0.7(1)	0.8(3)
Ni2 in 6 <i>c</i> (0, 0, <i>z</i>)		
<i>z</i>	0.3335(2)	0.3334(4)
<i>U</i> _{iso} × 100 (Å ²)	0.13(8)	1.8(3)
Ni3 in 18 <i>h</i> (<i>x</i> , − <i>x</i> , <i>z</i>)		
<i>x</i>	0.5009(3)	0.5014(6)
<i>z</i>	0.08529(8)	0.0854(2)
<i>U</i> _{iso} × 100 (Å ²)	0.57(5)	1.4(2)
R-factors of refinements		
<i>R</i> _p	8.9	7.4
<i>R</i> _{wp}	11.9	9.6
χ^2	2.0	2.1
Impurity phases		
	LaNi ₅ 7.8(2) wt%	LaNi ₅ 20.5(2) wt%
	MgNi ₂ 12.0(2) wt%	MgNi ₃ 4.2(3) wt%

The crystallographic characteristics of LaNi₃ change significantly on Mg → La substitution; a decrease in the unit cell parameters takes place from *a* = 5.0842(2); *c* = 25.106(1) Å (LaNi₃) to *a* = 4.8986(1) (sample 2)-4.94024(8) (sample 1); *c* = 23.8188(4) Å (sample 1)-23.957(1) (sample 2). Furthermore, comparison of the data shows that the studied intermetallic samples exhibit significant differences in the volumes of the unit cells and *c/a* ratios. A shrinkage along [001] appears to be more pronounced ($\Delta c/c$, −5.1%) as compared to $\Delta a/a$, −3.7%. The overall volume contraction is quite significant reaching 10.5%–11.5%. The measured dimensions of the unit cells well agree with the data reported for the stoichiometric LaMg₂Ni₉ alloy studied by single crystal XRD (*a* = 4.9241, *c* = 23.875 Å; *V* = 501.3 Å³ [15]), which shows intermediate values of *a*, *c* and *V* being in between the values for the samples 1 and 2, as it could be expected from comparison of their chemical compositions.

Refined volumes of the unit cells correlate with their chemical compositions and Mg/La ratios. Indeed, sample 1, $\text{La}_{1.09(1)}\text{Mg}_{1.91(1)}\text{Ni}_9$ with a larger unit cell has a higher content of lanthanum, while for sample 2, $\text{La}_{0.91(1)}\text{Mg}_{2.09(1)}\text{Ni}_9$ with a smaller unit cell, the content of lanthanum becomes smaller than 1 atom/f.u., and the content of Mg reaches overstoichiometric compositions with more than 2 Mg atoms/f.u. $(\text{La},\text{Mg})_3\text{Ni}_9$.

Comparison of the data presented in Table 1 with crystallographic data for the $(\text{La},\text{Mg})_3\text{Ni}_9$ intermetallics studied in [1] shows a linear dependence between the decrease of the unit cell volumes and the content of Mg in the alloys.

We note a very interesting feature of the crystal structure of $\text{La}_{0.91(1)}\text{Mg}_{2.09(1)}\text{Ni}_9$ where a partial substitution of La by Mg takes place within the CaCu_5 type layer in the position 6c. This contrasts with the behaviour of the alloys in the La-Mg-Ni system with compositions close to LaNi_5 . In the latter case studies of phase equilibria showed no dissolution of an appreciable amount of Mg in LaNi_5 [16]. Thus, the present study demonstrates that the situation with Mg solubility in the LaNi_5 slabs of the LaNi_3 structure becomes different in the sample 2 $\text{La}_{0.91(1)}\text{Mg}_{2.09(1)}\text{Ni}_9$. Here LaNi_5 , when influenced by the MgNi_2 slabs of the hybrid structure, becomes capable of forming solid solutions of such a type with experimentally refined composition of $\text{La}_{0.95}\text{Mg}_{0.05}\text{Ni}_5$. Thus, $\text{La}_{0.91(1)}\text{Mg}_{2.09(1)}\text{Ni}_9$ should be considered as the first reported case where a CaCu_5 type layer accommodates Mg atoms allowing a Mg content of 2.09 at./f.u. $(\text{La},\text{Mg})_3\text{Ni}_9$. Consequently, the limits of Mg solubility in LaNi_3 are not confined to LaMg_2Ni_9 and extend to the composition $\text{La}_{0.91}\text{Mg}_{2.09}\text{Ni}_9$.

3.2. Thermodynamics of the $(\text{La},\text{Mg})_3\text{Ni}_9\text{—H}_2$ systems

The hydrogenation/deuteration properties of the prepared $\text{La}_{1\pm 0.1}\text{Mg}_{2\pm 0.1}\text{Ni}_9$ intermetallics appear to be dramatically different from those for LaNi_3 . While LaNi_3 is prone to the hydrogen-induced disproportionation, the Mg-containing intermetallics reversibly form hydrides with $\Delta H_{\text{des}} = 24.0 \text{ kJ/mol}_{\text{H}_2}$ and equilibrium pressure of H_2 desorption of 20 bar at room temperature for $\text{La}_{1.09}\text{Mg}_{1.91}\text{Ni}_9$ (see Figure 2). A pronounced hysteresis of H_2 absorption and desorption is evidenced by a high value of H_2 absorption pressure, more than 100 bar higher than that for desorption.

For La_2MgNi_9 [6] at room temperature the values of plateau pressures are 0.05 and 0.1 bar for hydrogen desorption and absorption, respectively, $\Delta H_{\text{des}} = 35.9 \text{ kJ/mol}_{\text{H}_2}$. Equilibrium pressure of hydrogen desorption for $\text{La}_{0.91}\text{Mg}_{2.09}\text{Ni}_9$ is by more than 1000 times higher than that for La_2MgNi_9 .

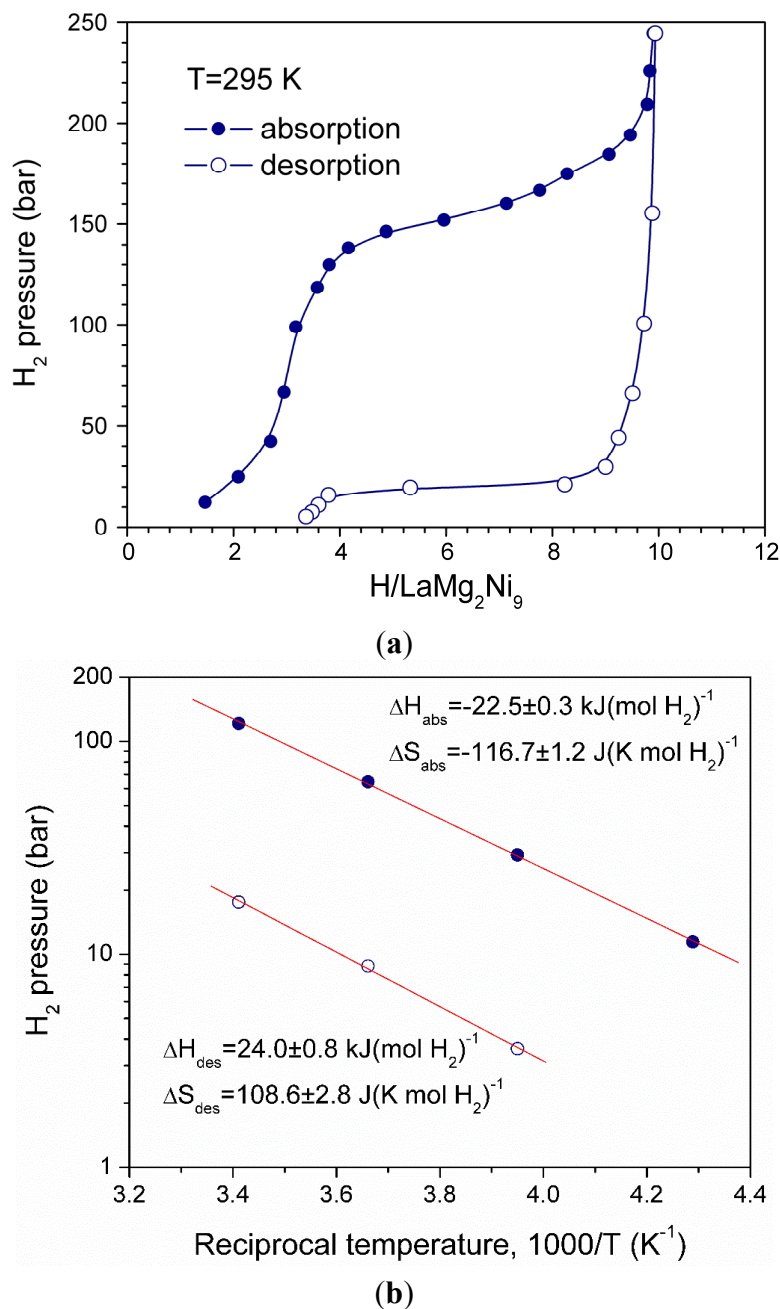


Figure 2. Room temperature isotherms of hydrogen absorption and desorption (a); and van't Hoff plots (b) for $\text{La}_{1.09}\text{Mg}_{1.91}\text{Ni}_9$ -based hydride. At room temperature equilibrium pressure of hydrogen absorption is ~ 120 bar D_2 , while for the desorption $P_{eq.}$ equals to ~ 20 bar D_2 .

3.3. In situ NPD studies

In situ neutron powder diffraction studies of the $\text{La}_{1\pm 0.1}\text{Mg}_{2\pm 0.1}\text{Ni}_9\text{D}_{9.4-9.5}$ deuterides were performed at the Spallation Neutron Source SINQ accommodated at Paul Scherrer Institute (Villigen, Switzerland). Two samples, $\text{La}_{1.09}\text{Mg}_{1.91}\text{Ni}_9\text{D}_{9.5(3)}$ (sample 1) and $\text{La}_{0.9}\text{Mg}_{2.1}\text{Ni}_9\text{D}_{9.4(6)}$ (sample 2) were synthesised and studied under different conditions.

For the synthesis of $\text{La}_{1.09}\text{Mg}_{1.91}\text{Ni}_9\text{D}_{9.5}$, a 6 mm diameter stainless steel autoclave with a wall thickness of 0.2 mm was used. The synthesis was performed by saturating activated samples with

deuterium gas (25 bar) at a sub-zero temperature of $-30\text{ }^{\circ}\text{C}$. This was done in order to decrease the equilibrium pressure of hydrogen absorption-desorption in the $\text{La}_{1.09}\text{Mg}_{1.91}\text{Ni}_9\text{—D}_2$ system. The alloy absorbed deuterium to reach a composition $\text{La}_{1.09}\text{Mg}_{1.91}\text{Ni}_9\text{D}_{9.5}$ and was measured at $25\text{ }^{\circ}\text{C}$ and deuterium pressure of 25 bar.

The second sample, $\text{La}_{0.9}\text{Mg}_{2.1}\text{Ni}_9\text{D}_{9.4}$, was synthesized at high pressure deuterium gas of 950 bar D_2 . The studied sample was placed inside a TiZr sample cell with a stainless steel liner, which was used as a sample holder during the *in situ* NPD experiments (see Figure 3). The pressure during the NPD measurements performed at $20\text{ }^{\circ}\text{C}$ was set to 912 bar D_2 . No preliminary activation was applied prior to the synthesis.

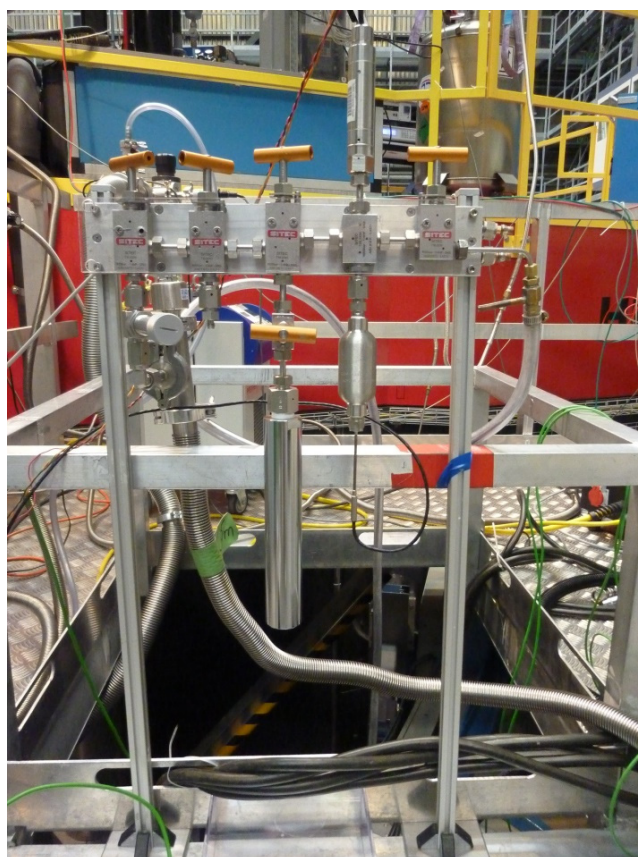


Figure 3. High pressure synthesis setup for the *in situ* NPD measurements at pressures up to 1000 bar D_2 .

For the $\text{La}_{1.09}\text{Mg}_{1.91}\text{Ni}_9\text{D}_{9.5(5)}$ sample (No.1) at the highest applied deuterium pressure of 25 bar D_2 , the deuteration resulted in the formation of a two-phase mixture of the α -solid solution of deuterium in the alloy and a corresponding β -deuteride. Such a mixture of the phase constituents was observed after allowing a deuteration time of ~ 20 h at interaction temperature of $-30\text{ }^{\circ}\text{C}$. Since applied temperature-pressure conditions were rather close to the equilibrium ones (see Figure 2), the transformation was slow and was not completed on the time scale of the measurements performed. The second sample with a slightly higher content of magnesium, $\text{La}_{0.91}\text{Mg}_{2.09}\text{Ni}_9\text{D}_{9.3(7)}$ was saturated by deuterium at deuterium pressure of 950 bar and was equilibrated at 912 bar D_2 and $25\text{ }^{\circ}\text{C}$. Analysis of the diffraction pattern showed an excellent fit between the experimental data and calculated NPD profiles (Figure 4) and indicated a completeness of the transformation of the α -solid solution into the β -deuteride.

The results of the refinements of the NPD data for $\text{La}_{1.09}\text{Mg}_{1.91}\text{Ni}_9\text{D}_{9.5(5)}$ and for $\text{La}_{0.91}\text{Mg}_{2.09}\text{Ni}_9\text{D}_{9.4(6)}$ are summarized in Table 2. The data show a formation of very similar structures, with only minor differences in the occupancies of the specific D-sites of five various types. These sites are shown in Figure 5 and include four types of tetrahedral and one tetragonal bipyramid.

A partial filling by D atoms of the four types of the tetrahedral interstices takes place inside the MgNi_2 slab; these include two types of the $[\text{MgNi}_3]$ (18*h* and 6*c*) tetrahedra and two types of the $[\text{Mg}_2\text{Ni}_2]$ (36*i* and 18*h*) interstitial sites.

In addition, similar to the other studied $\text{La}_{3-x}\text{Mg}_x\text{Ni}_9$ -based deuterides, the remaining 5.0 or 5.6 at. D/f.u. form a standard hydrogen sublattice within the LaNi_5 slab which are statistically distributed within the four types of the interstices; hydrogen atoms partially occupy $[\text{La}_2\text{Ni}_4]$ octahedra, three types of $[\text{Ni}_4]$ tetrahedra, and two types of the $[\text{LaMgNi}_2]$ sites.

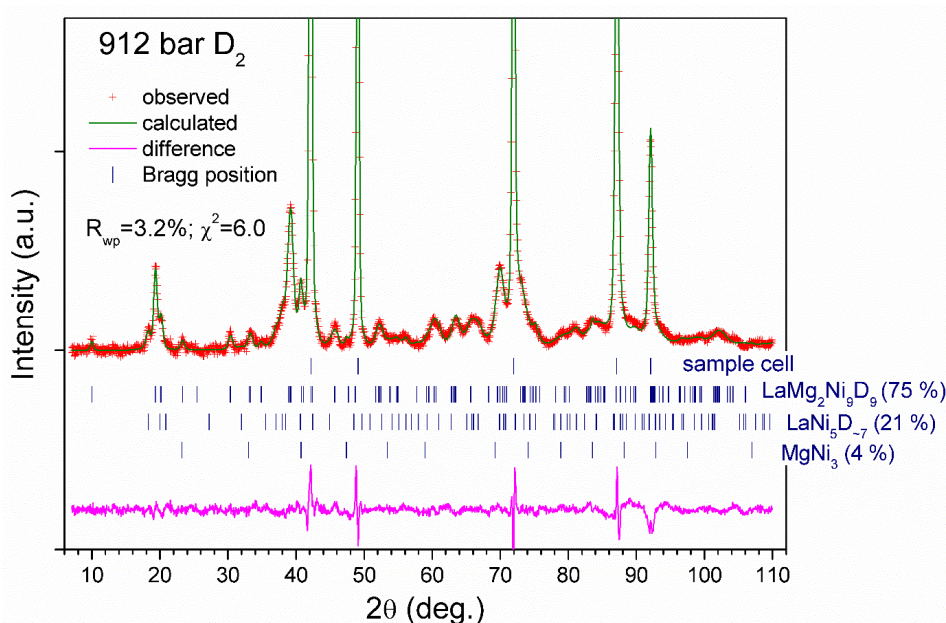


Figure 4. NPD pattern of $\text{La}_{0.9}\text{Mg}_{2.1}\text{Ni}_9\text{D}_{9.4(6)}$ (912 bar D_2 , 298 K). Note that the most significant contributions to the difference intensities are coming from the sample cell. $R_p = 2.4\%$, $R_{wp} = 3.2$; $\chi^2 = 6.0$.

Table 2. Crystal structure data for the deuterated $\text{La}_{1\pm 0.1}\text{Mg}_{2\pm 0.1}\text{Ni}_9$ alloys (PuNi_3 type, sp.gr. $R\bar{3}m$) from the Rietveld refinements of *in situ* neutron diffraction data.

Deuteride	$\text{La}_{1.09}\text{Mg}_{1.91}\text{Ni}_9\text{D}_{9.5(5)}$	$\text{La}_{0.91}\text{Mg}_{2.09}\text{Ni}_9\text{D}_{9.4(6)}$
Conditions	25 bar at 25 °C (prepared at −30 °C)	912 bar at 25 °C
Unit cell parameters:		
<i>a</i> (Å)	5.263(1)	5.212(1)
<i>c</i> (Å)	25.803(9)	25.71(1)
<i>V</i> (Å ³)	618.9(3)	604.8(3)

Table 2. Cont.

Deuteride	La _{1.09} Mg _{1.91} Ni ₉ D _{9.5(5)}	La _{0.91} Mg _{2.09} Ni ₉ D _{9.4(6)}
Unit cell parameters:		
$\Delta a/a$ (%)	6.5	6.4
$\Delta c/c$ (%)	8.3	7.3
$\Delta V/V$ (%)	23.0	21.6
$\Delta V/V[\text{LaNi}_5]$ (%)	20.4	20.7
$\Delta V/V[\text{MgNi}_2]$ (%)	25.4	22.2
Atomic parameters:		
La1/Mg1 in 3a (0, 0, 0)	0.0(–)	0.09(–)
n_{Mg} , ($n_{\text{La}} = 1 - n_{\text{Mg}}$)		
La2/Mg2 in 6c (0, 0, z)		
z	1.0(–)	1.0(–)
$U_{\text{iso}} \times 100$ (Å ²)	0.95(–)	1.0(–)
n_{Mg} , ($n_{\text{RE}} = 1 - n_{\text{Mg}}$)		
Ni1 in 3b (0, 0, 1/2)	1.0(–)	1.0(–)
$U_{\text{iso}} \times 100$ (Å ²)		
Ni2 in 6c (0, 0, z)	0.3279(7)	0.3220(6)
z	1.0(–)	1.0(–)
$U_{\text{iso}} \times 100$ (Å ²)		
Ni3 in 18h (x, –x, z)	0.498(1)	0.506(1)
x	0.0871(4)	0.0859(3)
z	1.0(–)	1.0(–)
$U_{\text{iso}} \times 100$ (Å ²)		
D1 in 18h (x, –x, z)	0.484(4)	0.496(3)
x	0.023(1)	0.023(1)
z	0.33(1)	0.31(2)
n		
D2 in 6c (0, 0, z)	0.390(1)	0.385(1)
z	0.50(3)	0.58(3)
n		
D4' in 18h (x, –x, z)	0.814(3)	0.792(2)
x	0.0626(9)	0.051(1)
z	0.43(2)	0.33(3)
n		
D5' in 18h (x, –x, z)	0.201(2)	0.192(3)
x	0.120(1)	0.123(1)
z	0.45(2)	0.35(2)
n		
D6 in 18h (x, –x, z)	0.819(4)	0.819(4)
x	0.117(1)	0.117(1)
z	0.20(2)	0.39(2)
n		
$U_{\text{iso}} \times 100$ (Å ²) for D1-D6	2.0(–)	2.0(–)

Table 2. Cont.

Deuteride	La _{1.09} Mg _{1.91} Ni ₉ D _{9.5(5)}	La _{0.91} Mg _{2.09} Ni ₉ D _{9.4(6)}
Atomic parameters:		
D distribution in the structure	5.6(3)	5.0(4)
LaNi ₅	3.9(2)	4.4(2)
2 MgNi ₂		
Shortest Metal—Hydrogen distances, Å		
La...D	2.34(3)	2.29(2)
Mg...D	1.97(3)	1.93(2)
Ni...D	1.56(3)	1.53(2)
<i>R</i> -factors of refinements		
<i>R</i> _p	2.7	2.4
<i>R</i> _{wp}	3.4	3.2
χ^2	5.0	6.0
Secondary constituents	<p>α-solid solution <u>La_{0.9}Mg_{2.1}Ni₉D_{0.9}</u>. Sp.gr. $R\bar{3}m$; $a = 4.9459(2)$; $c = 23.842(2)$ Å; $V = 505.10(4)$. 0.3 D in D3 18h (0.15, 0.3, 0.085) and 0.6 D in D4 18h (0.3, 0.15, 0.085); 35.7(2) wt% <u>LaNi₅D₇</u>; Sp.gr. $P6_3mc$; $a = 5.438(3)$, $c = 8.598(5)$ Å; $V = 220.3(2)$ Å³; 4.6(3) wt%.</p> <p>Atomic structure was taken from [3]. <u>MgNi₂</u>; MgNi₂ structure type; Sp.gr. $P6_3/mmc$; $a = 4.8356(4)$, $c = 15.850(3)$ Å; $V = 320.97(5)$ Å³; 12.4(2) wt%.</p> <p>Atomic structure was taken from [4]. <u>Sample holder</u>: stainless steel; Sp.gr. $Fm\bar{3}m$; $a = 3.598$ Å.</p>	<p><u>LaNi₅D₇</u>; Sp.gr. $P6_3mc$; $a = 5.430(1)$, $c = 8.606(4)$ Å; $V = 219.8(2)$ Å³; 21.5(5) wt%.</p> <p>Atomic structure was taken from [3]. <u>MgNi₃</u>; AuCu₃ structure type; Sp.gr. $Pm\bar{3}m$; $a = 3.7185$ Å; 1 Mg in 1a: 0, 0, 0; 3 Ni in 3c: 1/2, 1/2, 0; 3.7(2) wt%.</p> <p>Sample holder: zero matrix TiZr alloy with Fe liner. The peaks from Fe liner are only observed. Sp.gr. $Fm\bar{3}m$; $a = 3.5949(1)$ Å.</p>

From the refinements of the NPD data we conclude that the overall chemical compositions La_{1.09}Mg_{1.91}Ni₉D_{9.5}/La_{0.91}Mg_{2.09}Ni₉D_{9.4} can be presented as LaNi₅H_{5.6}/LaNi₅H_{5.0} + 2*MgNi₂H_{1.95}/MgNi₂H_{2.2}. Thus, in the hybrid La_{1±0.1}Mg_{2±0.1}Ni₉ structure, a LaNi₅-assisted hydrogenation of the MgNi₂ slab proceeds at rather mild H₂/D₂ pressure conditions; the equilibrium D₂ desorption pressure is just 20 bar D₂. In contrast, the parent MgNi₂ intermetallic remains inert with respect to hydrogenation even at much higher hydrogen pressures as well as the conditions applied in the present study of 912 bar D₂ for sample 2.

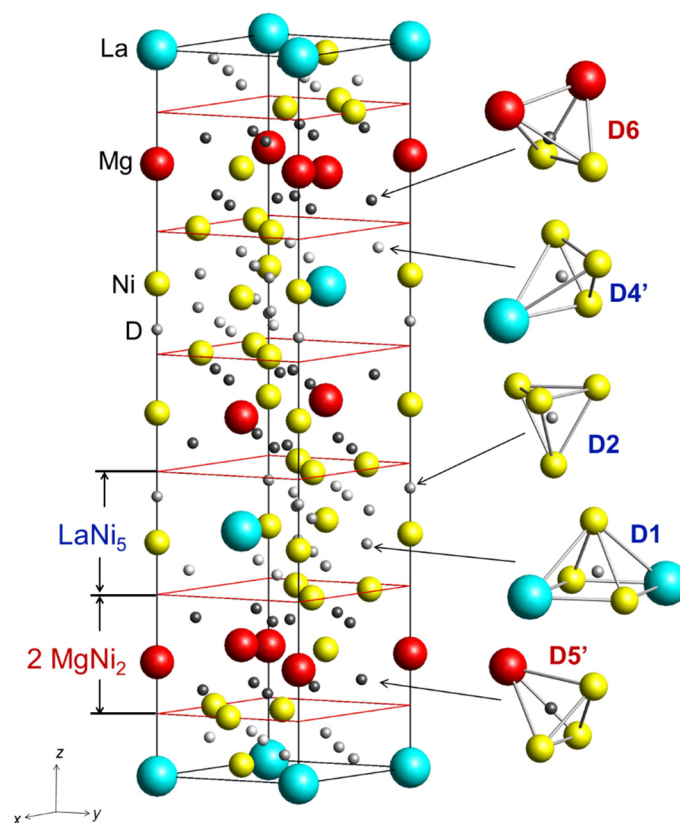


Figure 5. Crystal structure of $\text{La}_{1\pm 0.1}\text{Mg}_{2\pm 0.1}\text{Ni}_9\text{D}_{9.4-9.5}$ and types of the filled interstices.

The shortest Me–D distances in the studied deuterides are listed in Table 2 and are within the regular values for the La–H, Mg–H and Ni–H distances in the structures of the metal and intermetallic hydrides.

The data of the present study clearly shows an influence of the LaNi_5 and MgNi_2 layers in the hybrid $\text{La}_{1\pm 0.1}\text{Mg}_{2\pm 0.1}\text{Ni}_9$ structures on the hydrogenation of the other buildings blocks of the structure. MgNi_2 slabs accommodate hydrogen up to a composition $\text{MgNi}_2\text{H}_{2.2}$ at much lower pressures as compared to those required to form a hydride by the pure MgNi_2 intermetallic. In contrast, the LaNi_5 block absorbs 5.0–5.6 at.H/f.u., which is quite close to the maximum hydrogenation capacity of the title intermetallic alloy, LaNi_5H_7 ; however, hydrogen desorption from the $\text{LaNi}_5\text{H}_{5.0/5.6}$ block proceeds much easier, at significantly higher pressures of H_2/D_2 as compared to the individual LaNi_5H_7 hydride—as a result of influence of the MgNi_2 slab.

4. Conclusions

LaNi_5 -assisted hydrogenation of MgNi_2 is observed in the LaMg_2Ni_9 hybrid structure. Formation of $\text{LaMg}_2\text{Ni}_9\text{D}_{9.5}$ proceeds via an *isotropic* expansion of the trigonal unit cell. D atoms are accommodated in both Laves and CaCu_5 -type slabs H atoms filling interstitial sites in both LaNi_5 and MgNi_2 structural fragments.

Limits of Mg solubility in LaNi_3 are not confined to LaMg_2Ni_9 and extend to the composition $\text{La}_{0.91}\text{Mg}_{2.09}\text{Ni}_9$ with a refined composition of the CaCu_5 -type block of $\text{La}_{0.95}\text{Mg}_{0.05}\text{Ni}_5$.

Within the LaNi_5 CaCu_5 -type layer, D atoms fill three types of interstices; a deformed octahedron $[\text{La}_2\text{Ni}_4]$, and two types of tetrahedra, $[\text{LaNi}_3]$ and $[\text{Ni}_4]$, to yield $\text{LaNi}_5\text{D}_{5-5.6}$ composition. D distribution is very similar to that in the individual $\beta\text{-LaNi}_5\text{D}_7$ deuteride.

In the MgNi_2 slab hydrogen atoms fill two types of tetrahedra, $[\text{Mg}_2\text{Ni}_2]$ and $[\text{MgNi}_3]$. The hydrogen sublattice formed is unique and is not formed in the studied structures of the Laves-type intermetallic hydrides.

A significant mutual influence of the LaNi_5 and MgNi_2 slabs causes a dramatic altering of their hydrogenation behaviours leading to:

- (a) significant decrease of the stability of the LaNi_5 -type hydride;
- (b) much easier hydrogenation of the MgNi_2 slabs compared to the parent intermetallic compound;
- (c) increased hysteresis.

Acknowledgments

This work received support from the Research Council of Norway (project 223084 NOVELMAG “NOVEL MAGNESIUM BASED NANOMATERIALS FOR ADVANCED RECHARGEABLE BATTERIES”) and is a part of the activities within the IEA Task32 “Hydrogen Based Energy Storage”. The skillful assistance from the staff of the Swiss-Norwegian Beam Lines during the experimental studies at ESRF is gratefully acknowledged. Denis Sheptyakov (PSI, Switzerland) is sincerely thanked for the collaboration in the neutron powder diffraction experiments at HRPT, PSI (experiments 20090547, 20101348 and 20110612).

Author Contributions

All authors contributed extensively to the work presented in this paper. Volodymyr A. Yartys supervised the project. Evan MacA. Gray and Colin J. Webb designed and built the high pressure 1000 bar rig. Roman V. Denys, Volodymyr A. Yartys and Colin J. Webb jointly performed the in situ neutron powder diffraction experiments, while Roman V. Denys analyzed the NPD data. Roman V. Denys and Evan MacA. Gray measured the PCT diagrams. Volodymyr A. Yartys wrote the paper. All authors discussed the results and commented on the manuscript at all stages.

Conflicts of Interest

The authors declare no conflict of interest.

References

1. Denys, R.V.; Yartys, V.A. Effect of magnesium on crystal structure and thermodynamics of the $\text{La}_{3-x}\text{Mg}_x\text{Ni}_9$ hydrides. *J. Alloys Compd.* **2011**, *509* (Suppl. 2), S540–S548, doi:10.1016/j.jallcom.2010.11.205.
2. Denys, R.V.; Yartys, V.A.; Webb, C.J. LaNi_5 -assisted hydrogenation of MgNi_2 in the hybrid structure of $\text{LaMg}_2\text{Ni}_9\text{D}_{9.5}$. In Proceedings of the International Symposium on Metal-Hydrogen Systems MH2012, Fundamental and Applications, Kyoto, Japan, 21–26 October 2012; Poster Presentation. MoP38. Collected Abstracts. P.92.
3. Lartigue, C.; Percheron Guégan, A.; Achard, J.C.; Soubeyroux, J.L. Hydrogen (deuterium) ordering in the $\beta\text{-LaNi}_5\text{D}_x$ phases: A neutron diffraction study. *J. Less-Common. Met.* **1985**, *113*, 127–148, doi:10.1016/0022-5088(85)90155-9.

4. Yartys, V.A.; Antonov, V.E.; Beskrovnyi, A.I.; Crivello, J.-C.; Denys, R.V.; Fedotov, V.K.; Gupta, M.; Kulakov, V.I.; Kuzovnikov, M.A.; Latroche, M.; *et al.* Hydrogen assisted phase transition in a trihydride MgNi_2H_3 synthesised at high H_2 pressures: thermodynamics, crystallographic and electronic structures. *Acta Mater.* **2015**, *82*, 316–327, doi:10.1016/j.actamat.2014.09.012.
5. Denys, R.V.; Yartys, V.A.; Webb, C.J. Hydrogen in $\text{La}_2\text{MgNi}_9\text{D}_{13}$. The role of magnesium. *Inorg. Chem.* **2012**, *51*, 4231–4238, doi:10.1021/ic202705u.
6. Nwakwuo, C.C.; Holm, T.H.; Denys, R.V.; Hu, W.; Maehlen, J.P.; Solberg, J.K.; Yartys, V.A. Effect of magnesium content and quenching rate on the phase structure and composition of rapidly solidified La_2MgNi_9 metal hydride battery electrode alloy. *J. Alloys Compd.* **2013**, *555*, 201–208, doi:10.1016/j.jallcom.2012.12.017.
7. Hu, W.-K.; Denys, R.V.; Nwakwuo, C.C.; Holm, T.H.; Maehlen, J.P.; Solberg, J.K.; Yartys, V.A. Annealing effect on phase composition and electrochemical properties of the Co-free La_2MgNi_9 anode for Ni-Metal Hydride batteries. *Electrochim. Acta* **2013**, *96*, 27–33, doi:10.1016/j.electacta.2013.02.064.
8. Latroche, M.; Cuevas, F.; Hu, W.-K.; Sheptyakov, D.; Denys, R.V.; Yartys, V.A. Mechanistic and kinetic study of the electrochemical charge and discharge of La_2MgNi_9 by *in situ* powder neutron diffraction. *J. Phys. Chem. C* **2014**, *118*, 12162–12169, doi:10.1021/jp503226r.
9. Gabis, I.E.; Evard, E.A.; Voyt, A.P.; Kuznetsov, V.G.; Tarasov, B.P.; Crivello, J.-C.; Latroche, M.; Denys, R.V.; Hu, W.; Yartys, V.A. Modeling of metal hydride battery anodes at high discharge current densities. *Electrochim. Acta* **2014**, *147*, 73–81, doi:10.1016/j.electacta.2014.08.107.
10. Yartys, V.A.; Denys, R.V. Structure-properties relationship in $\text{RE}_{3-x}\text{Mg}_x\text{Ni}_9\text{H}_{10-13}$ (RE = La, Pr, Nd) hydrides for energy storage. *J. Alloys Compd.* **2015**, doi:10.1016/j.jallcom.2014.12.091.
11. Yartys, V.A.; Denys, R.V. Thermodynamics and crystal chemistry of the $\text{RE}_2\text{MgNi}_9\text{H}_{12-13}$ (RE=La and Nd) hydrides. *Chem. Met. Alloys* **2014**, *7*, 1–8.
12. Larson, A.C.; Dreele, R.B.V. General structure analysis system (GSAS). In *Los Alamos National Laboratory Report LAUR*, 2000; Alamos National Lab, Los Alamos, NM, USA, 2000; pp. 86–748.
13. Rodríguez-Carvajal, J. Recent advances in magnetic structure determination by neutron powder diffraction. *Phys. B: Condens. Matter* **1993**, *192*, 55–69, doi:10.1016/0921-4526(93)90108-I.
14. Liu, G.; Xi, S.; Ran, G.; Zuo, K.; Li, P.; Zhou, J. A new phase MgNi_3 synthesized by mechanical alloying. *J. Alloys Compd.* **2008**, *448*, 206–209, doi:10.1016/j.jallcom.2006.10.068.
15. Kadir, K.; Yamamoto, H.; Sakai, T.; Uehara, I.; Kanehisa, N.; Kai, Y.; Eriksson, L. LaMg_2Ni_9 , an example of the new AB_2C_9 structure type. *Acta Crystallogr.* **1999**, *C55*, doi:10.1107/S0108270199098418.
16. De Negri, S.; Giovannini, M.; Saccone, A. Phase relationships of the La–Ni–Mg system at 500 °C from 66.7 to 100 at% Ni. *J. Alloys Compd.* **2005**, *397*, 126–134, doi:10.1016/j.jallcom.2006.08.236.